

REVISITING THE Fe XVII LINE EMISSION PROBLEM: HIGH-RESOLUTION LABORATORY MEASUREMENTS OF THE $3s - 2p$ AND $3d - 2p$ LINE-FORMATION CHANNELS

CHINTAN SHAH^{1,*}, JOSÉ R. CRESPO LÓPEZ-URRUTIA¹, MING FENG GU², THOMAS PFEIFER¹, JOSÉ MARQUES^{3,4}, FILIPE GRILO⁴,
JOSÉ PAULO SANTOS⁴, AND PEDRO AMARO^{4,*}

¹Max-Planck-Institut für Kernphysik, D-69117 Heidelberg, Germany

²Space Science Laboratory, University of California, Berkeley, CA 94720, USA

³University of Lisboa, Faculty of Sciences, BioISI - Biosystems & Integrative Sciences Institute, Lisboa, Portugal and

⁴Laboratório de Instrumentação, Engenharia Biomédica e Física da Radiação (LIBPhys-UNL),
Departamento de Física, Faculdade de Ciências e Tecnologia, FCT, Universidade Nova de Lisboa, 2829-516 Caparica, Portugal

Draft version February 10, 2022

ABSTRACT

We determined relative X-ray photon emission cross sections in Fe XVII ions that were mono-energetically excited in an electron beam ion trap. Line formation for the $3s - 2p$ and $3d - 2p$ transitions of interest proceeds through dielectronic recombination (DR), direct electron-impact excitation (DE), resonant excitation (RE), and radiative cascades. By reducing the electron-energy spread to a sixth of that of previous works and increasing counting statistics by three orders of magnitude, we account for hitherto unresolved contributions from DR and the little-studied RE process to the $3d - 2p$ transitions, and also for cascade population of the $3s - 2p$ line manifold through forbidden states. We found good agreement with state-of-the-art many-body perturbation theory (MBPT) and distorted-wave (DW) method for the $3s - 2p$ transition, while in the $3d - 2p$ transitions known discrepancies were confirmed. Our results show that DW calculations overestimate the $3d - 2p$ line emission due to DE by $\sim 20\%$. Inclusion of electron-electron correlation effects through the MBPT method in the DE cross section calculations reduces this disagreement by $\sim 11\%$. The remaining $\sim 9\%$ discrepancy is consistent with those found in previous laboratory measurements, solar, and astrophysical observations. Meanwhile, spectral models of opacity, temperature, and turbulence velocity should be adjusted to these experimental cross sections to optimize the accuracy of plasma diagnostics based on these bright soft X-ray lines of Fe XVII.

Keywords: atomic data — atomic processes — line: formation — methods: laboratory: atomic — plasmas — X-rays: general

1. INTRODUCTION

Soft X-rays spectra from astrophysical hot plasmas at a few MK are recorded by grating spectrometers onboard the *Chandra* and *XMM-Newton* X-ray observatories. They are dominated by the L -shell $3d - 2p$ and $3s - 2p$ transitions in the 15–17 Å range from Fe XVII (Ne-like ions) (Paerels & Kahn 2003; Canizares et al. 2000) that are used for electron temperature, density (Mewe et al. 2001; Behar et al. 2001; Xu et al. 2002; Beiersdorfer et al. 2018), velocity turbulence, and X-ray opacity diagnostics (Brickhouse & Schmelz 2005; Werner et al. 2009; Sanders et al. 2011; de Plaa et al. 2012; Kallman et al. 2014). Decay from the states $[2p_{1/2}^5 3d_{3/2}]_{J=1}$, $[2p_{3/2}^5 3d_{5/2}]_{J=1}$, and $[2p_{3/2}^5 3d_{3/2}]_{J=1}$ to the $[2p_{1/2}^6]_{J=0}$ ground state produces the $3d - 2p$ transitions called $3C$, $3D$, and $3E$, respectively. The $3s - 2p$ decays known as $3F$, $3G$, and $M2$ lines proceed from $[2p_{1/2}^5 3s_{1/2}]_{J=1}$, $[2p_{3/2}^5 3s_{1/2}]_{J=1}$, and $[2p_{1/2}^5 3s_{1/2}]_{J=2}$, also to $[2p_{1/2}^6]_{J=0}$.

Since the optically thick line $3C$ and the intercombination line $3D$ both have low contributions from cascades (Mewe et al. 2001), their intensity ratio mainly depends on direct electron impact excitation (DE) and dielectronic recombination (DR) processes. The diagnostic utility of this ratio is limited by discrepancies between observations (e. g., the recent Bernitt et al. (2012)) and various predictions of their oscillator and collision strengths, which can lead to overestimating opacity effects (Parkinson 1973; Brown et al. 1998; Lam-

ing et al. 2000; Beiersdorfer et al. 2002, 2004; Brown et al. 2006; Chen 2007; Liang & Badnell 2010; Gillaspy et al. 2011; Bernitt et al. 2012). While nonlinear effects in certain scenarios could also reduce the $3C/3D$ ratio (Oreshkina et al. 2014; Loch et al. 2015), and in spite of forty years of efforts, the $3C/3D$ collision-strength discrepancy remains essentially unsolved (Chen 2011; Santana et al. 2015; Mendoza & Bautista 2017; Wang et al. 2017).

Alternative approaches use the forbidden $M2$ line or the $3G + M2$ line blend for opacity, and turbulence-velocity diagnostics, since the $M2$ line is optically thinner than the $3D$ line (de Plaa et al. 2012; Werner et al. 2009). However, astrophysical observations of the $(3G + M2)/3C$ ratio and $3s/3d$ or $(3F + 3G + M2)/(3C + 3D + 3E)$ ratio also depart from spectral models (de Plaa et al. 2012), and laboratory ratios are consistently larger than the calculated ones (Beiersdorfer et al. 2002, 2004). This could be explained if $M2$ is mainly fed by complex cascades following DE, with contributions from resonant excitation (RE) (Beiersdorfer et al. 1990; Doron & Behar 2002; Gu 2003; Tsuda et al. 2017). Another argument points to the same cause than the $3C/3D$ discrepancy. Thus, laboratory validation of calculations of the DR, DE, and RE contributions to these transitions is essential to construct reliable spectral models, and urgently needed in view of the upcoming high-resolution space missions *XRISM Resolve* (Tashiro et al. 2018), *Arcus* (Smith et al. 2016), and *Athena* (Barret et al. 2016).

In this Letter, we perform calculations both distorted-wave (DW) and many-body perturbation theory (MBPT) of the Fe XVII $3s$ ($3F + 3G + M2$) and $3d$ ($3C + 3D + 3E$) emissions

* chintan@mpi-hd.mpg.de
* pdamaro@fct.unl.pt

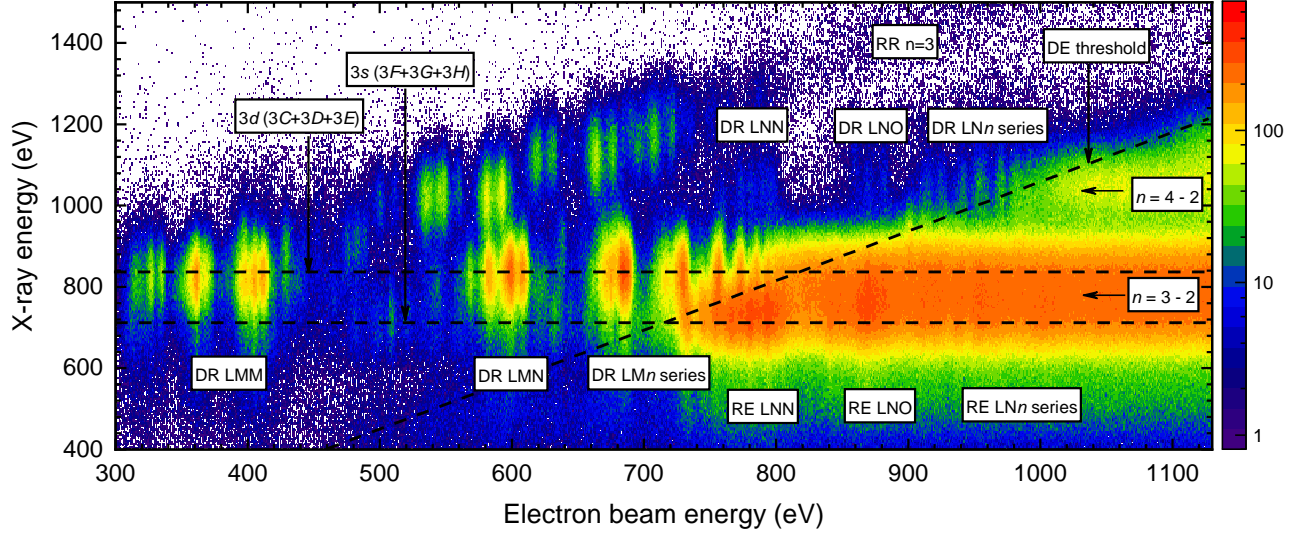


Figure 1. Measured X-ray flux in dependence of photon (3.7 eV/bin) and electron energy (0.9 eV/bin). Bright DR and RE resonances are labeled by their respective dielectronic capture channel and can contribute as unresolved satellites to the $3d-2p$ ($3C+3D+3E$) and $3s-2p$ ($3F+3G+M2$) transition groups marked by horizontal dashed lines.

driven by DR, DE, and RE. Further, we measure their differential cross sections in the 0.3–1.1 keV energy range using an electron beam ion trap (EBIT), reducing the electron energy spread to only 5 eV full-width-at-half-maximum (FWHM), and distinguishing narrow RE and DR features from DE ones. Except for the $3d$ cross sections, we found overall agreement with both DW and MBPT predictions. Our results confirm previous work indicating that a fundamental discrepancy in $3d$ formation causes the reported inconsistencies of models with laboratory and astrophysical observations.

2. EXPERIMENTAL TECHNIQUE

We used FLASH-EBIT (Epp et al. 2010) at the Max-Planck-Institut für Kernphysik in Heidelberg to produce Fe XVII ions from a molecular beam of iron pentacarbonyl. The monoenergetic electron beam induces a negative space-charge potential that radially traps the ions; in the axial direction, a set of cylindrical drift tubes electrostatically confines them. In the trap, the electrons have a well defined kinetic energy due to the acceleration potentials corrected by the space-charge contributions of electron beam and trapped ions. Collisions between beam electrons and trapped ions efficiently drive ionization, excitation, and recombination processes. The generated X-rays are registered at 90° to the beam axis with a silicon-drift detector (SDD) with a photon-energy resolution of ≈ 120 eV FWHM at 6 keV, which separate transitions from the $3s$ and $3d$ manifolds, see Fig. 1.

To maximize Fe XVII purity, a saw-tooth scan consists of an breeding time of 0.5 s at 1.15 keV beam energy (below the Fe XVII ionization threshold at 1.26 keV), followed by a 40 ms-long energy scan from 0.3 keV to 1.1 keV during which only a small fraction of the ions recombine. This method efficiently suppressed lower charge states, as only very faint LMM DR resonances from Fe XV–XVI are obtained. Measurements at a breeding energy of 0.5 keV, just above the Fe XVI ionization threshold allowed us to separately identify those weak contributions. The DR paths are named in analogy to Auger nomenclature, e.g., LMM implies an $L \rightarrow M$ resonant excitation due to a free electron recombining into the M -shell. Moreover, the spectra taken on the upward and

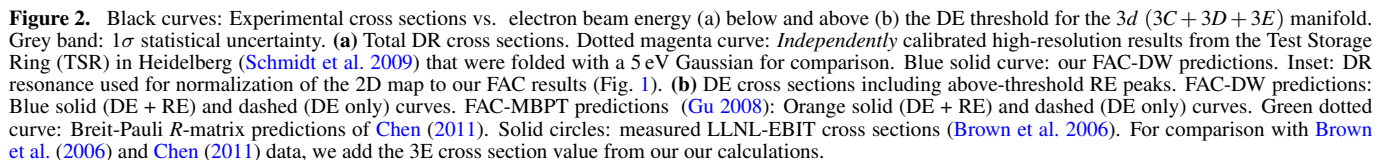
downward energy scans show differences of less than 2% and confirm a nearly constant population of Fe XVII ions. We reached an electron-beam energy spread of ~ 5 eV FWHM at 800 eV, six times smaller than in previous work in this energy range (Brown et al. 2006; Beiersdorfer et al. 2017) by applying evaporative cooling (Penetrante et al. 1991). During the fast energy scans, the beam current I_e was also adjusted synchronously with E to keep the electron density $n_e \propto I_e/\sqrt{E}$ constant (Savin et al. 2000), minimizing a modulation of the space-charge potential, and concomitant heating that causes ion losses. The trap was emptied every 5 s to prevent accumulation of unwanted (Ba, W) ions emanating from the electron-gun cathode.

3. THEORY

Within an independent resonance approximation model, the DR and RE processes can be described as a two-step process, shown in Eq. 1. First, a doubly excited state is formed by dielectronic capture (DC), i.e., a capture of a free electron by an ion with excitation of a bound electron. Here, we focus on the L -shell. While in DR this excited state decays radiatively, RE includes an autoionization process which leaves a L -shell hole that relaxes by photon emission.

We used the parallel version of Flexible Atomic Code³ (FAC v1.1.5) (Gu 2008) with to compute the electronic structures of Fe XVII–XVI ions. We evaluated DR, DE, and RE with extended sets of configurations, full-order configuration mixing, and Breit interaction. For the DC channels of both DR and RE, as well as for DE and cascades, we included $2s^2 2p^5 n l n' l'$ and $2s 2p^6 n l n' l'$ configurations with $n \leq 7$, $n' \leq 60$ and $l, l' < 8$, or roughly half-a-million eigenstates. All the DR radiative paths of these states were included, which corresponds to the main radiative recombination (RR) paths. Additionally, all Auger paths addressing RE were account for. They are also the main pathways of DE as shown in Eq. 1. The output was fed into the collisional-radiative model of FAC for obtaining steady-state populations of Fe XVII–XVI states connected by the aforementioned processes and radiative cas-

³ <https://github.com/flexible-atomic-code/fac>



Various paths between these configurations are depicted in Eq. 1,

For the DE cross sections, we used the MBPT implementation of FAC. The treatment of DE with MBPT is described by Gu (2009). In essence, a combined configuration interaction and second-order MBPT method (Gu et al. 2006) is used to refine the energy levels and multipole transition matrix elements. Collision strengths of DE under the DW ap-

Due to the unidirectional electron beam and the side-on X-ray observation, both polarization and emission anisotropy must be accounted for (Beiersdorfer et al. 1996; Shah et al. 2015). We used also FAC to calculate the X-ray polarization following DR, DE, and RE. Depolarization due to radiative cascades and cyclotron motion of the electrons was taken into account (Gu et al. 1999; Shah et al. 2018). The latter resulted into a negligible effect.

Figure 1 shows the X-ray intensity as a function of the electron beam (abscissa) and the X-ray energies (ordinate). Features due to electron recombination can be recognized above and below the DE threshold. Above it, we resolve DR channels populating the $3d$ manifold from LMM to LMT , while unresolved LMn DR channels up to $n > 60$ pile up near the $3d$ threshold. Below threshold, photon emission produced af-

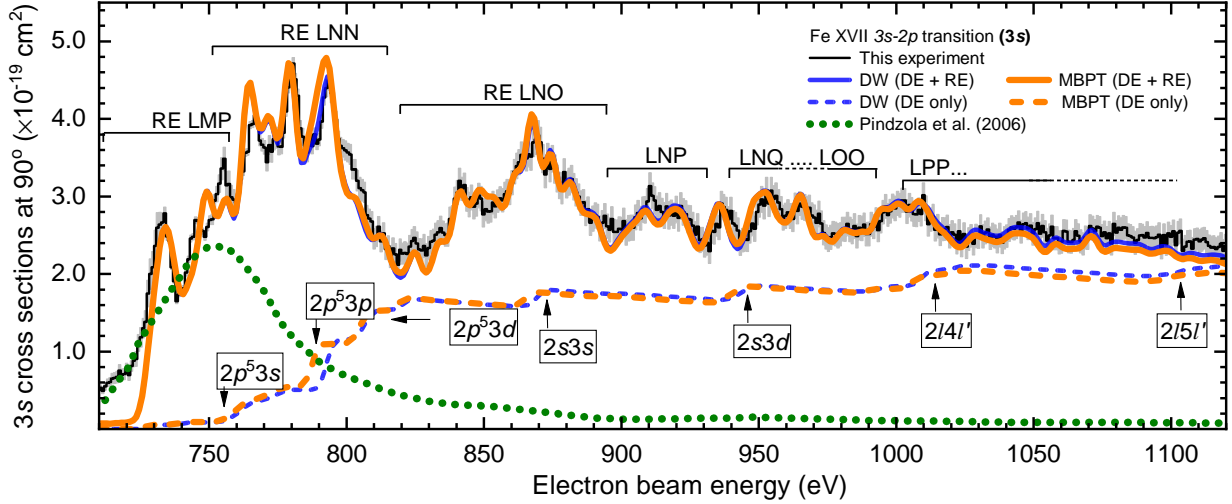


Figure 3. Same as in Fig. 2b, except for the 3s or ($3F + 3G + M2$) manifold. Green dotted line: 30-eV broadened $2p^5 3s$ cross sections from Pindzola et al. (2006).

ter DE of L -shell electrons appears as horizontal bright band comprising both the $3d$ and $3s$ manifolds. Bright spots on top of the continuous DE emission band in Fig. 1 are RE features.

Two horizontal regions of interest (ROI) with an X-ray energy width of ± 30 eV and centered on the respective line centroids were carefully selected on the 2D map for distinguishing the contributions of the $3s$ and $3d$ manifolds. The X-ray photon count within these ROIs were projected onto the electron-energy axis, see Figs. 2 and 3. In front of the windowless SDD detector, a $1\mu\text{m}$ carbon foil blocks UV light from the trapped ions. At the X-ray energies of interest varying from 650 to 900 eV, the foil has a transmission of 26–52%. We normalized counts with known transmission coefficients (Henke et al. 1993). To verify them, we carried out measurements of $\text{Ly}\alpha$ and radiative recombination (RR) emissions from O VIII and Ne X, and found them in agreement within 3%. Furthermore, X-ray yields were also normalized to the cyclically time-varying electron beam current density. After that we determine the relative differential cross sections.

Previously, Brown et al. (2006), using a X-ray microcalorimeter calibrated their experiment with theoretical RR cross sections, and determined the $3C$ and $3D$ cross sections. This was not possible here due to pile-up and contamination of the RR band, since the detector does not resolve RR transitions into the $3s$, $3p$ and $3d$ sub-shells. We thus selected a single DR resonance, $[1s^2 2s^2 2p_{1/2} 3d_{3/2} 3d_{5/2}]_{7/2}$ at ~ 412 eV electron beam energy, see the inset of the Fig. 2, for a calibration also based on theory. Its intensity can be traced to a single, and strong resonance in the LMM channel. This channel has the simplest structure of all DR channels and this makes its prediction presumably more reliable. By fitting the experimental spectra and the theoretical one (convoluted with a Gaussian function), a calibration factor of 1.42×10^{21} counts per cm^2 with a 2% fitting error was found. The complete spectrum was accordingly rescaled, yielding the differential cross sections for both the $3d$ and $3s$ manifolds.

To further ascertain our calibration, we used the DR rate coefficients measured at the Test Storage Ring (TSR) at the Max-Planck-Institut für Kernphysik in Heidelberg by the merged-beam method. There, a cooled Fe XVII ion beam is brought to overlap with an electron beam as electron target (Schmidt et al. 2009). The yield of Fe XVI, not X-ray

photons, is detected, resulting in a high-resolution, absolute total recombination-rate coefficient that we re-scale to a cross section and convolute to a 5 eV Gaussian for the comparison. In the Fig. 2, the *independently* calibrated TSR data are shown along our own. Both agree within 2% for the calibration DR resonance we used. This is indeed a reassuring; although, the quoted uncertainty in the *non-theory-based* TSR DR rates is 20% (Schmidt et al. 2009). Moreover, our data also agree with the cross sections measured at the LLNL-EBIT by Brown et al. (2006) at 910 eV and 964 eV energies. This overall agreement of three independent experiments is shown in Fig. 2a and 2b.

We further checked the effect of the $3s$ - $3d$ ROI selection, since even though our detector resolves them, the wings of both transitions partially overlap. This is evident in Fig. 1: the low energy tail of $3d$ peak contaminates the $3s$ manifold. To check those blends, we shifted the $3s$ and $3d$ ROIs up to ± 15 eV from their respective centroids, leading to effects on the calibration factor of 9%. This adds a $\sim 9\%$ uncertainty to our calibration factor, in addition to the $\sim 2\%$ uncertainty from the LMM fits. Uncertainty sources are thus: $\sim 2\%$ from statistics, $\sim 3\%$ from the carbon-foil transmission, and $\sim 9\%$ from the calibration factor. Note that our calibration is based on a single theoretical value.

The resulting cross sections of DR, RE, and DE for $3d$ and $3s$ are shown in Figs. 2 and 3, respectively, and compared with FAC-MBPT and FAC-DW predictions.

5. RESULTS AND DISCUSSIONS

Overall, we observe agreement over a wide range of electron energies. However, a few discrepancies are noticeable. The comparison of TSR DR data with the current experiment in Fig. 2a shows minor differences in the baseline, since for clarity the contributions to the total cross section from $n = 4 - 2$ photon emission that are visible in the 2D plot at ~ 1 keV photon energies (see Fig. 1) were left out, while they are present in the TSR data. The TSR data do not include DE and RE processes, thus its signal disappears above the threshold at 0.8 keV.

Another discrepancy in Fig. 3 at electron energies of 0.72 keV could not be attributed to the $3s$ ROI selection or contamination by a DR feature at 0.83 keV photon en-

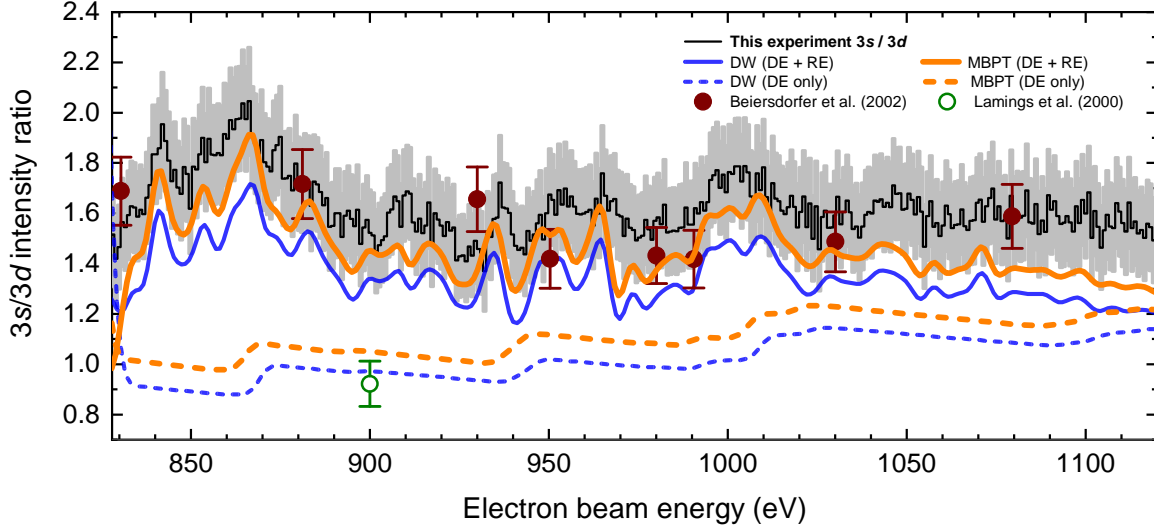


Figure 4. Measured $3s$ ($3F + 3G + M2$) to $3d$ ($3C + 3D + 3E$) line intensity ratios as a function of the electron beam energy. Black curve: present experiment. Grey shaded area: 1σ statistical error. Solid circles: LLNL-EBIT microcalorimeter (Beiersdorfer et al. 2002). Open circles: SAO microcalorimeter (Laming et al. 2000). Blue solid and dashed curves show distorted-wave (DW) predictions that include (DE + RE) and exclude RE (DE only), respectively. Similarly, orange solid and dashed curves show the many-body perturbation theory (MBPT) predictions.

Table 1
Experimental and theoretical values of the integral cross sections ($10^{-18} \text{ cm}^2 \text{ eV}$) for the $3s$ and $3d$ manifolds and their dimensionless ratio. The predicted contributions of various processes from DW and MBPT calculations are compared with experimental values.

Line	E_e range (eV)	Integral cross sections (in $10^{-18} \text{ cm}^2 \text{ eV}$)				% Contribution of processes		% MBPT correction	% Required correction	
		This exp.	DW Theory		MBPT Theory	DW theory		to DW theory	to theory	
			DE + RE	DE only	DE only	% RE	% DE		DE only	DW
$3s$	710 - 1120	110.6 ± 5.7	108.29	60.82	60.35	43.8	56.2	-0.8	2.2	2.6
$3d$	830 - 1120	47.6 ± 4.2	57.19	52.69	47.56	7.9	92.1	-10.8	-20.1	-9.4
$3s/3d$	830 - 1120	1.64 ± 0.17	1.35	1.02	1.11	24.6	75.4	8.0	17.5	10.6

ergy. Calculations assuming 10% of Fe XVI, five times the predicted concentration based on comparison of upward and downward scans, still predict a negligible contribution of Fe XVI at this energy. Furthermore, Fe XVII DR channel ($2p^5 3snl$) calculations also predict negligible contributions at 0.72 keV.

We further checked contamination by oxygen ions producing Ly β and Ly γ lines. These contributions were estimated by exciting KLL DR resonances of O VII-V in the electron-energy range of 0.42–0.55 keV, which is free from low-energy tail contamination from Fe XVII DR resonances, see Fig. 1. We found out less than 1% counts could be due to O KLL DR, compared to the strong Fe LMM features, ruling out this source of discrepancy.

The $3s$ emission in Fig. 3 shows a dominant contribution of RE in the proximity of the excitation threshold (0.73–0.8 keV) of the total photon emission. This can be traced back to the LMP ($2p^5 3l6l'$) and LNN ($2p^5 4l4l'$) resonances. Previously, Pindzola et al. (2006) predicted the LMP RE contribution to the $2p^5 3s$ DE cross section at ≈ 750 eV. In addition to this, we observe RE channels up to LPP ($2l6l'6l''$), which are necessary to fully understand our data up to $E \approx 0.11$ keV. Furthermore, DE processes populate states having non-dipole (e.g. $2p^5 3p$) decays to the ground state, feeding the $3s$ manifold through radiative cascades. The excitation thresholds of such states are apparent in the stepwise shape of the non-RE theoretical prediction in Fig. 3. Excellent agreement is observed when all these atomic processes are taken into account

and compared with both DW and MBPT theoretical methods. Table 1 lists theoretical and experimental total cross sections, as well as the contribution of RE and DE, showing detailed agreement between both theories and experiment for the $3s$ manifold.

On the other hand, the $3d$ emission shown in Fig. 2b and its total cross section in Table 1 demonstrate an overestimation of DW theory by 20%, while MBPT overpredicts by only 9%. Such differences also appear in earlier predictions (Chen & Pradhan 2002; Loch et al. 2006; Chen 2007, 2008, 2011). For example, previous predictions for the $3d$ cross sections reported by Loch et al. (2006) and Chen & Pradhan (2002) differ by 14% and 17% from our measurements, respectively. The difference between our present MBPT and experiment is likely due to the $3C$ component of the $3d$ manifold (see Fig. 7 of Gu (2009)). As discussed by Chen (2007); Gu (2009); Chen (2011); Santana et al. (2015), the main difference between theoretical methods evaluating the $3C$ component can be traced back to the completeness of electron correlation, and not to the theoretical scattering implementation, i. e., regardless of using DW, close-coupling, or R-matrix methods. The MBPT-corrected cross sections presented here give a better agreement with the measurements because of their more complete treatment of correlation effects in comparison with our DW cross sections. We note that the remaining discrepancy on the $3C$ component indicates that higher-order correlation effects beyond second order need to be considered (Safronova et al. 2001), as also confirmed in the earlier findings (Bernitt et al. 2012). Laboratory measurements (Brown et al. 2006)

performed at the LLNL-EBIT are within our uncertainties (see Fig. 2), and share the same conclusion that the actual 3C cross sections are lower than theoretical predictions. Here, we note that the present measurement resolved the RE components for the 3d manifold and found its overall contribution to be $\sim 8\%$.

The ratios of 3s to 3d cross sections, which are independent of calibration and are of astrophysical preeminence, plotted in Fig. 4 as a function of electron beam energies, are also in good agreement with the LLNL results of Beiersdorfer et al. (2002), but in disagreement with a microcalorimeter measurement of Laming et al. (2000). Similarly to the previous reasoning, we again find a better agreement with predictions having a more complete treatment of electron correlation for the 3C through the MBPT method.

6. SUMMARY AND CONCLUSIONS

In conclusion, we report a systematic measurement of the soft X-ray emission in Fe XVII after electron recombination with an much-improved electron energy resolution for both the 3s and 3d line manifolds. We ascertain that predictions have to include substantially larger sets of configurations and the corresponding contributions of DR and RE to the DE process, as well as the effect of forbidden transitions driving the line emission through cascades. Our DW and MBPT predictions show a good agreement with the measured 3s cross sections. On the other hand, the discrepancy for the 3d excitation found in earlier studies was broadly confirmed. The agreement between our measurements and previous laboratory data based on storage ring, ion trap, and tokamak measurements, and the reproducibility of the observed discrepancy in the 3d manifold, let us also conclude in accord with earlier work that the main disparities between models and astrophysical observations in the 3s/3d, 3C/3D, and 3C/(3G + M2) are due to an overestimation of the 3C component.

Our experimental data and dedicated calculations may contribute to a better understanding of these line ratios, which are used for estimating opacity and turbulence velocities in galaxies (de Plaa et al. 2012; Beiersdorfer et al. 2004). They can be used to benchmark widely-used spectral codes, such as SPEX (Kaastra et al. 1996) and ATOMDB (Foster et al. 2012). Validation of such codes is, indeed, an urgent task in view of the upcoming launch of the X-ray microcalorimeter-based *XRISM* satellite. The expected scientific harvest of this mission, and the future ones *Arcus* and *Athena* should revolutionize X-ray astrophysics, as the few but nonetheless, excellent measurements of the ill-fated *Hitomi* mission have shown.

7. ACKNOWLEDGEMENTS

We acknowledge Prof. Dr. Stefan Schippers for providing the raw data of dielectronic recombination rates measured at the Test Storage Ring. We also thank Dr. Zoltán Harman for valuable discussion on this work. P. A. acknowledges the support from Fundação para a Ciência e a Tecnologia (FCT), Portugal, under Grant No. UID/FIS/04559/2013(LIBPhys) and under Contract No. SFRH/BPD/92329/2013.

REFERENCES

- Barret, D., et al. 2016, *Proc. SPIE*, 9905, 99052F
 Behar, E., Cottam, J., & Kahn, S. M. 2001, *The Astrophysical Journal*, 548, 966

- Beiersdorfer, P., Bitter, M., Goeler, S. v., & Hill, K. W. 2004, *Astrophys. J.*, 610, 616
 Beiersdorfer, P., Brown, G. V., & Laska, A. 2017, *AIP Conference Proceedings*, 1811, 040001
 Beiersdorfer, P., Hell, N., & Lepson, J. K. 2018, *The Astrophysical Journal*, 864, 24
 Beiersdorfer, P., Osterheld, A. L., Chen, M. H., et al. 1990, *Phys. Rev. Lett.*, 65, 1995
 Beiersdorfer, P., Vogel, D. A., Reed, K. J., et al. 1996, *Phys. Rev. A*, 53, 3974
 Beiersdorfer, P., Behar, E., Boyce, K. R., et al. 2002, *Astrophys. J. Lett.*, 576, L169
 Bernitt, S., Brown, G. V., Rudolph, J. K., et al. 2012, *Nature*, 492, 225
 Brickhouse, N. S., & Schmelz, J. T. 2005, *The Astrophysical Journal*, 636, L53
 Brown, G. V., Beiersdorfer, P., Liedahl, D. A., Widmann, K., & Kahn, S. M. 1998, *Astrophys. J.*, 502, 1015
 Brown, G. V., Beiersdorfer, P., Chen, H., et al. 2006, *Phys. Rev. Lett.*, 96, 253201
 Canizares, C. R., Huenemoerder, D. P., Davis, D. S., et al. 2000, *Astrophys. J. Lett.*, 539, L41
 Chen, G.-X. 2007, *Phys. Rev. A*, 76, 062708
 —. 2008, *Phys. Rev. A*, 77, 022701
 Chen, G. X. 2011, *Phys. Rev. A*, 84, 012705
 Chen, G. X., & Pradhan, A. K. 2002, *Phys. Rev. Lett.*, 89, 013202
 de Plaa, J., Zhuravleva, I., Werner, N., et al. 2012, *A&A*, 539
 Doron, R., & Behar, E. 2002, *The Astrophysical Journal*, 574, 518
 Epp, S. W., López-Urrutia, J. R. C., Simon, M. C., et al. 2010, *J. Phys. B*, 43, 194008
 Foster, A. R., Ji, L., Smith, R. K., & Brickhouse, N. S. 2012, *Astrophys. J.*, 756, 128
 Gillasp, J. D., Lin, T., Tedesco, L., et al. 2011, *Astrophys. J.*, 728, 132
 Gu, M. F. 2003, *Astrophys. J.*, 582, 1241
 —. 2008, *Can. J. Phys.*, 86, 675
 Gu, M. F. 2009, arXiv e-prints, arXiv:0905.0519
 Gu, M. F., Holzer, T., Behar, E., & Kahn, S. M. 2006, *The Astrophysical Journal*, 641, 1227
 Gu, M. F., Savin, D. W., & Beiersdorfer, P. 1999, *J. Phys. B*, 32, 5371
 Henke, B. L., Gullikson, E. M., & Davis, J. C. 1993, *Atomic Data and Nuclear Data Tables*, 54, 181
 Kaastra, J. S., Mewe, R., & Nieuwenhuijzen, H. 1996, in *11th Colloq. on UV and X-ray Spectroscopy of Astrophysical and Laboratory Plasmas*, ed. K. Yamashita & T. Watanabe (Tokyo: Universal Academy Press), 411
 Kallman, T., Daniel, A. E., Marshall, H., et al. 2014, *Astrophys. J.*, 780, 121
 Laming, J. M., Kink, I., Takacs, E., et al. 2000, *Astrophys. J. Lett.*, 545, L161
 Liang, G. Y., & Badnell, N. R. 2010, *A&A*, 518, A64
 Loch, S. D., Ballance, C. P., Li, Y., Fogle, M., & Fontes, C. J. 2015, *Astrophys. J. Lett.*, 801, L13
 Loch, S. D., Pindzola, M. S., Ballance, C. P., & Griffin, D. C. 2006, *J. Phys. B*, 39, 85
 Mendoza, C., & Bautista, M. A. 2017, *Phys. Rev. Lett.*, 118, 163002
 Mewe, R., Raassen, A. J. J., Drake, J. J., et al. 2001, *A&A*, 368, 888
 Oreshkina, N. S., Cavaletto, S. M., Keitel, C. H., & Harman, Z. 2014, *Phys. Rev. Lett.*, 113, 143001
 Paerels, F. B. S., & Kahn, S. M. 2003, *Annual Review of Astronomy and Astrophysics*, 41, 291
 Parkinson, J. H. 1973, *Astron. Astrophys.*, 24, 215
 Penetrante, B. M., Bardsley, J. N., Levine, M. A., Knapp, D. A., & Marrs, R. E. 1991, *Phys. Rev. A*, 43, 4873
 Pindzola, M. S., Loch, S. D., Ballance, C. P., & Griffin, D. C. 2006, *Phys. Rev. A*, 73, 012718
 Safronova, U. I., Namba, C., Murakami, I., Johnson, W. R., & Safronova, M. S. 2001, *Phys. Rev. A*, 64, 012507
 Sanders, J. S., Fabian, A. C., & Smith, R. K. 2011, *Mon. Not. R. Astron. Soc.*, 410, 1797
 Santana, J. A., Lepson, J. K., Träbert, E., & Beiersdorfer, P. 2015, *Phys. Rev. A*, 91, 012502
 Savin, D. W., Beiersdorfer, P., Kahn, S. M., et al. 2000, *Rev. Sci. Instrum.*, 71, 3362
 Schmidt, E. W., Bernhardt, D., Hoffmann, J., et al. 2009, 163, 012028
 Shah, C., Amaro, P., Steinbrügge, R. e., et al. 2018, *Astrophys. J. Suppl. Ser.*, 234, 27
 Shah, C., Jörg, H., Bernitt, S., et al. 2015, *Phys. Rev. A*, 92, 042702
 Smith, R. K., Abraham, M. H., Allured, R., et al. 2016, in *Proc. SPIE, Vol. 9905, Space Telescopes and Instrumentation 2016: Ultraviolet to Gamma Ray*, 99054M
 Tashiro, M., Maejima, H., Toda, K., et al. 2018, *Proc. SPIE*, 10699, 1069922
 Tsuda, T., Shimizu, E., Ali, S., et al. 2017, *The Astrophysical Journal*, 851, 82
 Wang, K., Jönsson, P., Ekman, J. o. r., et al. 2017, *Phys. Rev. Lett.*, 119, 189301
 Werner, N., Zhuravleva, I., Churazov, E., et al. 2009, *Mon. Not. R. Astron. Soc.*, 398, 23
 Xu, H., Kahn, S. M., Peterson, J. R., et al. 2002, *Astrophys. J.*, 579, 600